SUPPORTING INFORMATION

Syndiotactic PLA from *meso*-LA polymerization at Al-chiral complex: a probe of DFT mechanistic insights.

Massimo Christian D'Alterio, Claudio De Rosa and Giovanni Talarico*

Dipartimento di Scienze Chimiche, Università degli Studi di Napoli Federico II, via Cintia, 80126 Napoli (Italy).

Corresponding authors: giovanni.talarico@unina.it

Table of Contents

1. Details of computational methods

All the DFT static calculations have been performed with the Gaussian09 set of programs,[1] using the B3LYP functional of Becke and Perdew.[2,3] The electronic configuration has been described with two different layers of basis set: 6-311G(d,p)[4] at the Al center to achieve a better description of the coordination geometry and SVP with the standard split-valence basis set with a polarization function of Ahlrichs and co-workers for H, C, N, and O.[5] Stationary points were characterized using vibrational analysis, and this analysis has been also used to calculate zero-point energies and thermal (enthalpy and entropy) corrections (298.15 K, 1 bar). We obtained improved electronic energies from single-point energy calculations using a 6-311G(d,p) basis set on all the atoms, a solvation contribute (PCM model,[6] toluene) and the dispersion corrections[7] (EmpiricalDispersion=GD3BJ in the Gaussian09 E.01 package). These energies added to the SVP-level thermal corrections are named ΔG. This computational protocol has been verified by test calculations optimizing the structures including the dispersion correction, but no significant changes in trend are observed with respect the optimization without dispersion. Additionally, the robustness of our theoretical approach has been already tested and all details are reported in the Supporting Information of reference 8.

The catalyst interconversion paths for **M3** mechanism reported in Fig. S2 have been calculated by freezing the O-Al-O angles at different values and optimizing the geometries; once we reached the maximum energetic path, we started for a real transition state (TS) search without constrains.

For each TS calculation of propagation steps, several chain conformations have been used to locate the lower energetic path. In the main text as well as in the Tables S1-S6 are reported the low-lying paths corresponding to the preferred LA enantioface and growing chains conformations.

Finally, we recall that systems **1**-(*R*) and **2**-(*R*) show different energetic values for *meso*-A versus *meso* B paths initiation reaction because of the difference of *meso*-LA insertion into -OCH_3 (as **1**-(*R*)) and -O^iPr bonds (as **2**-(*R*)), respectively. We calculated the Gibbs energy difference of these two paths also for system **2**-(*R*) in order to compare our prediction with the experimental results reported by Coates et al.[9] The calculated $\Delta\Delta G$ of 4.3 kcal/mol is in good agreement with the experimental results.[9] Furthermore, the close value of initiation (4.3 kcal/mol) and propagation (4.2 kcal/mol, see Table 5 of the main text,) nicely matches with the analogous experimental results for both initiation and propagation steps.

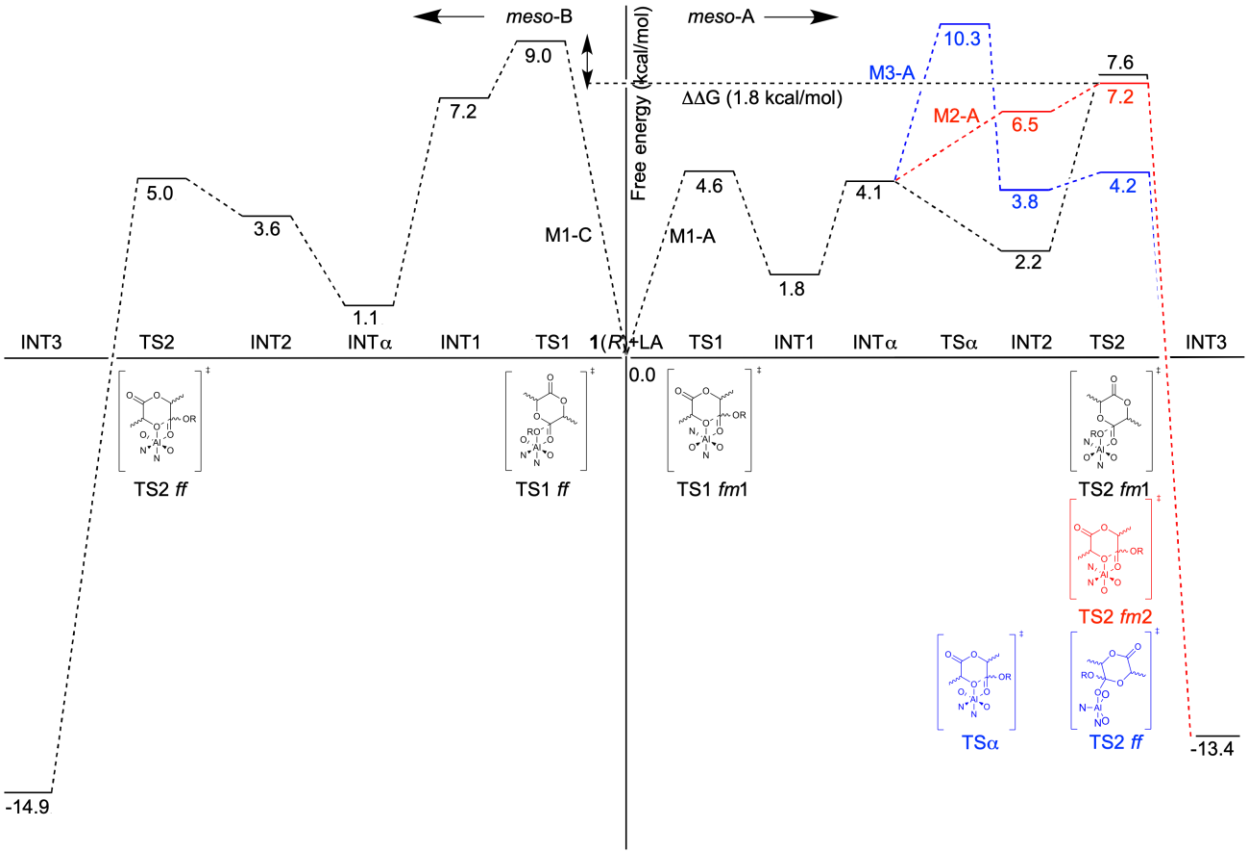

Fig. S1 Minimum energy paths for *meso*-A (right) and *meso*-B (left) initiation reaction at **1**-(R) system.

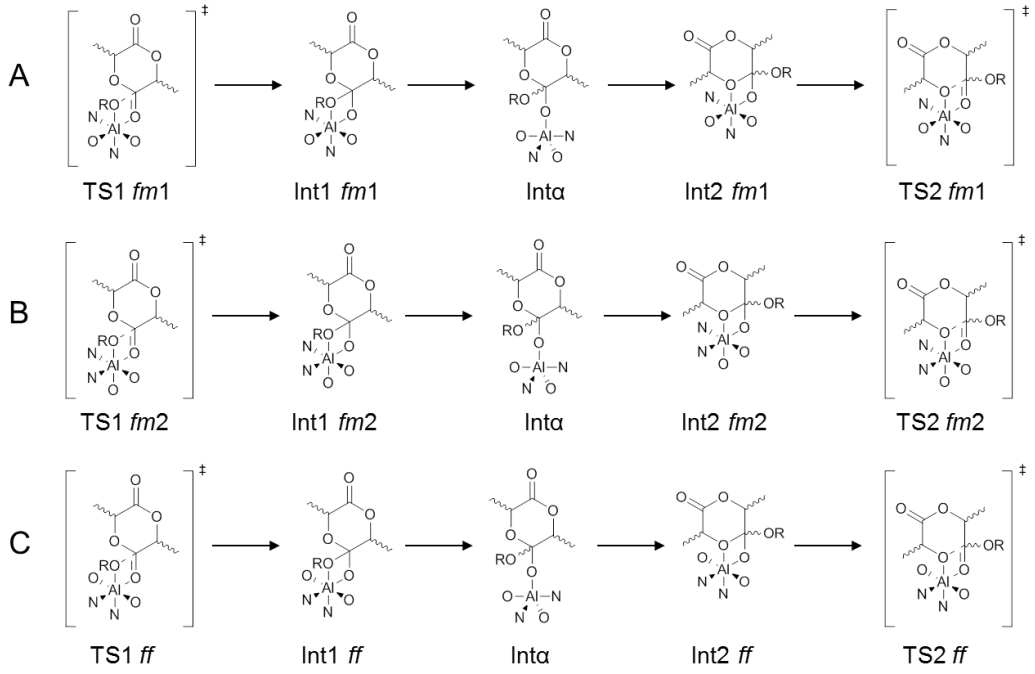

Scheme S1 The three different paths computed for the mechanism 1 (**M1**).

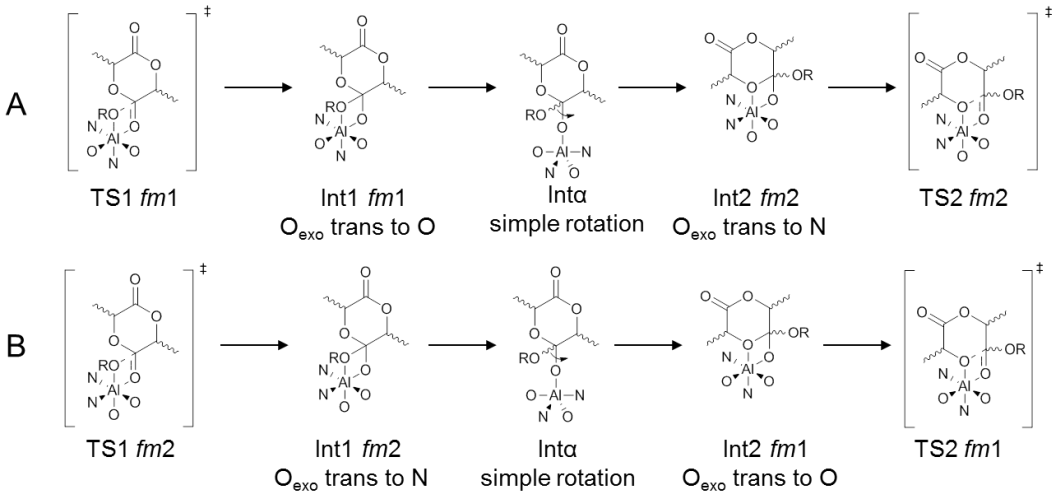

Scheme S2 The two different paths computed for the mechanism 2 (**M2**).

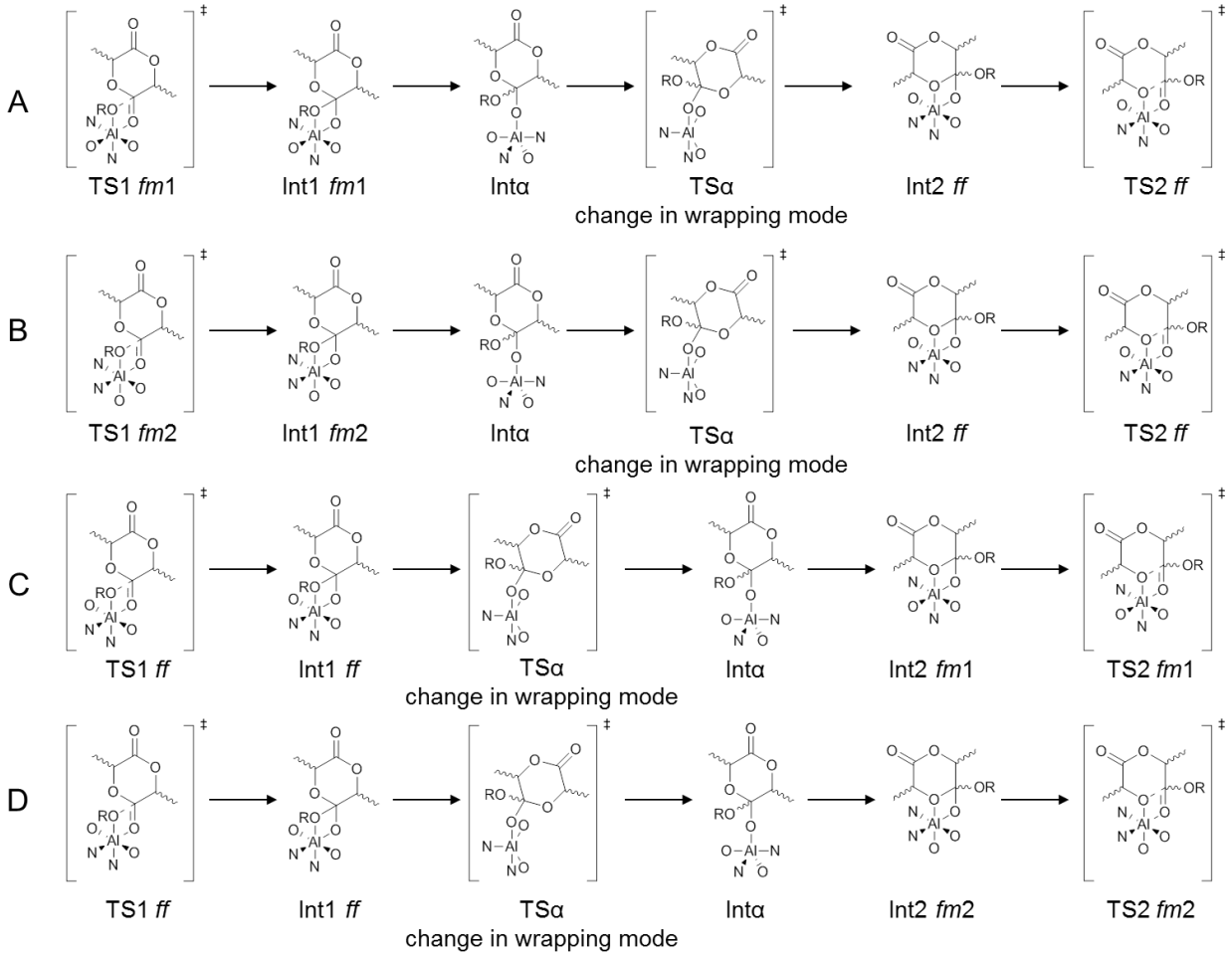

Scheme S3 The four different paths computed for the mechanism 3 **(M3)**.

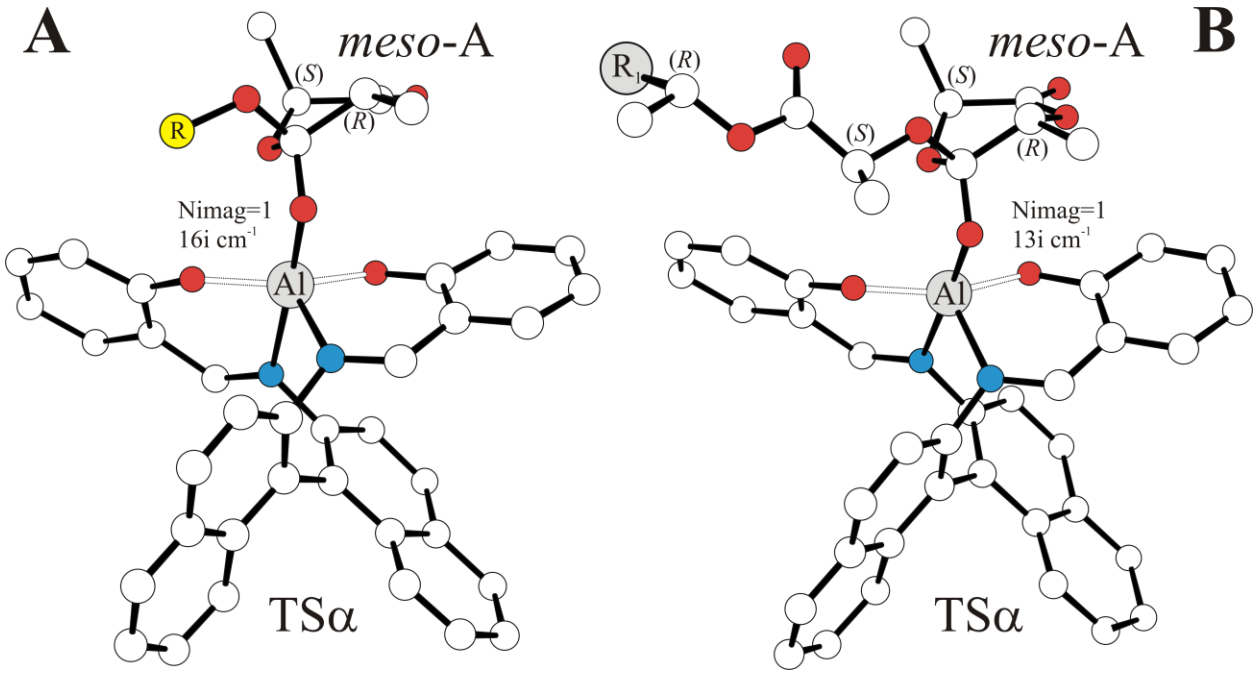

Fig. S2 DFT optimized geometries of *meso*-A TSα at **1**-(*R*) for the initiation reaction (**A**), with R = CH_3 and for propagation (**B**) with *meso*-A-chain (R_1 =$COOCH_3$). H atoms omitted for clarity, O and N atoms in red and blue,

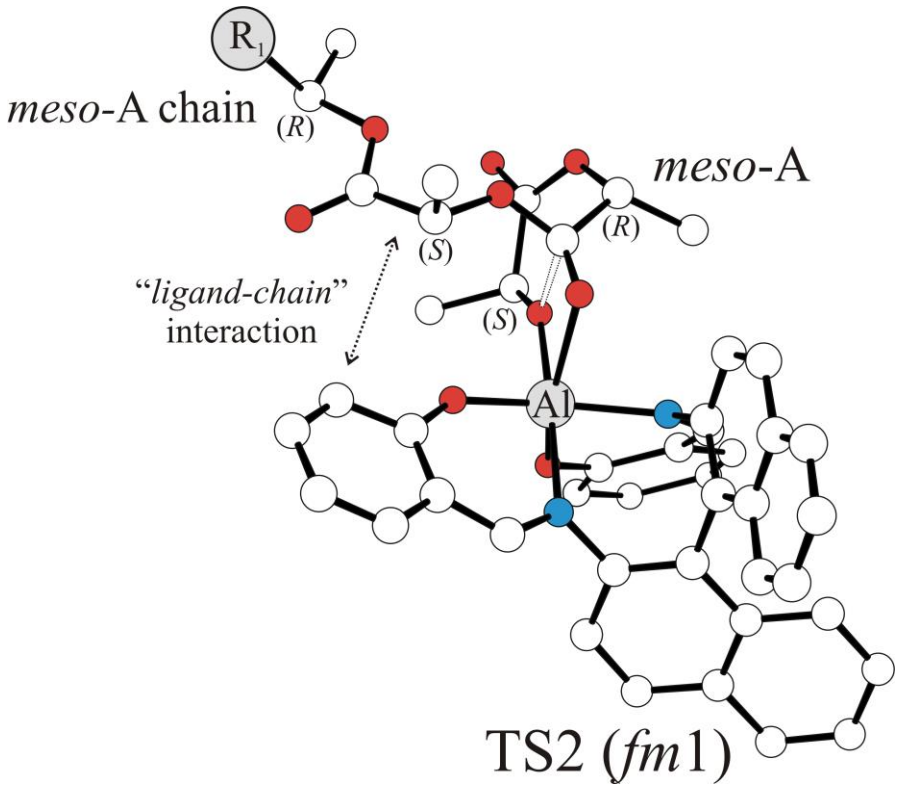

Fig. S3 DFT geometries for TS2 of *meso*-A at **1**-(*R*) with *fm*1 wrapping mode. H atoms omitted for clarity, O and N atoms in red and blue, R_1 =$COOCH_3$.

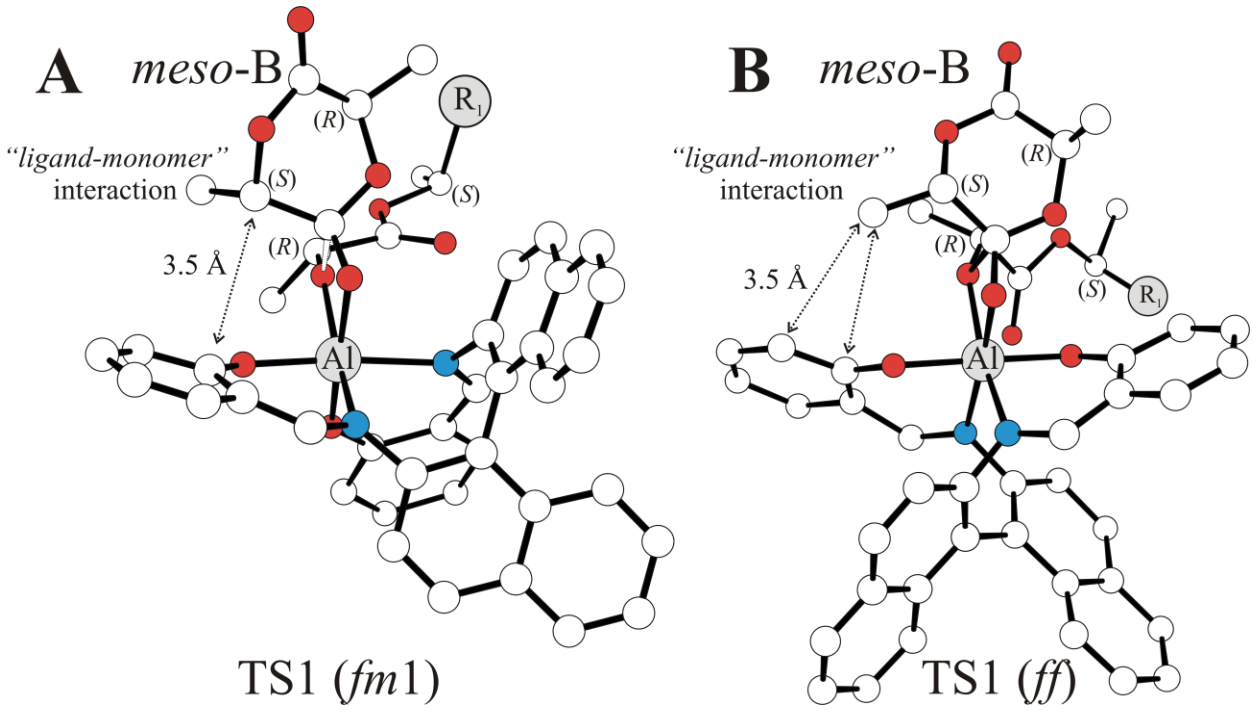

Fig. S4 DFT geometries for low-lying TS1 of *meso*-B at **1**-(*R*)-*meso*-B-chain with *fm*1 (**A**) and *ff* (**B**) wrapping mode, respectively. The distances between ligand and monomer C atom (*S*) (**A**) as well as methyl group linked to C atom (*S*) (**B**) are reported in Å. H atoms omitted for clarity, O and N atoms in red and blue, R_1 = $COOCH_3$.

Table S1 TSs free energies (Δ*G*, in kcal/mol) for all reaction paths computed for *meso*-A LA initiation reaction relative to **1**-(*R*)-OCH_3 + monomer. In red are reported the low-lying paths following the **M1**-**M3** mechanisms with the preferred *meso*-LA enantioface (see Fig. 2-B of the main text).

meso-A initiation reaction				
Mechanism 1 (**M1**)	Path	**TS1**		**TS2**
	A	4.6		7.6
	B	8.0		7.2
	C	8.0		4.2
Mechanism 2 (**M2**)		**TS1**		**TS2**
	A	4.6		7.2
	B	8.0		7.6
Mechanism 3 (**M3**)		**TS1**	**TSα**	**TS2**
	A	4.6	10.3	4.2
	B	8.0	10.3	4.2
	C	8.0	10.3	7.2
	D	8.0	10.3	7.6

Table S2. TSs free energies (Δ*G*, in kcal/mol) for all reaction paths computed for *meso*-B LA initiation reaction relative to **1**-(*R*)-OCH_3 + monomer. In red are reported the low-lying paths following the **M1**-**M3** mechanisms with the preferred *meso*-LA enantioface (see Fig. 2-B of the main text).

meso-B initiation reaction				
Mechanism 1 (**M1**)	Path	**TS1**		**TS2**
	A	9.4		8.8
	B	11.9		5.0
	C	9.0		5.0
Mechanism 2 (**M2**)		**TS1**		**TS2**
	A	9.4		5.0
	B	11.9		8.8
Mechanism 3 (**M3**)		**TS1**	**TSα**	**TS2**
	A	9.4	11.8	5.0
	B	11.9	11.8	5.0
	C	9.0	11.8	8.8
	D	9.0	11.8	5.0

Table S3. TSs free energies (Δ*G*, in kcal/mol) for all reaction paths computed for *meso*-A-LA propagation at **1-**(*R*)-*meso*-A-chain. In red are reported the low-lying paths following the **M1**-**M3** mechanisms with the preferred *meso*-LA enantioface (see Fig. 2-B of the main text).

meso-A propagation reaction at **1**-(*R*)-*meso*-A-chain				
Mechanism 1 (**M1**)	Path	**TS1**		**TS2**
	A	11.9		16.4
	B	20.2		13.9
	C	18.1		13.0
Mechanism 2 (**M2**)		**TS1**		**TS2**
	A	11.9		13.9
	B	20.2		16.4
Mechanism 3 (**M3**)		**TS1**	**TSα**	**TS2**
	A	11.9	15.7	13.0
	B	20.2	15.7	13.0
	C	18.1	15.7	16.4
	D	18.1	15.7	13.9

Table S4. TSs free energies (Δ*G*, in kcal/mol) for all reaction paths computed for *meso*-A-LA propagation at **1-**(*R*)-*meso*-B-chain. In red are reported the low-lying paths following the **M1**-**M3** mechanisms with the preferred *meso*-LA enantioface (see Fig. 2-B of the main text).

meso-A propagation reaction at **1**-(*R*)-*meso*-B-chain				
Mechanism 1 (**M1**)	Path	**TS1**		**TS2**
	A	13.4		14.7
	B	23.7		16.8
	C	19.3		11.3
Mechanism 2 (**M2**)		**TS1**		**TS2**
	A	13.4		16.8
	B	23.7		14.7
Mechanism 3 (**M3**)		**TS1**	**TSα**	**TS2**
	A	13.4	18.0	11.3
	B	23.7	18.0	11.3
	C	19.3	18.0	14.7
	D	19.3	18.0	16.8

Table S5. TSs free energies (Δ*G*, in kcal/mol) for all reaction paths computed for *meso*-B-LA propagation at **1-**(*R*)-*meso*-B-chain. In red are reported the low-lying paths following the **M1**-**M3** mechanisms with the preferred *meso*-LA enantioface (see Fig. 2-B of the main text).

meso-B propagation reaction at **1**-(*R*)-*meso*-B-chain				
Mechanism 1 (**M1**)	Path	**TS1**		**TS2**
	A	17.2		15.3
	B	26.6		12.6
	C	18.4		12.0
Mechanism 2 (**M2**)		**TS1**		**TS2**
	A	17.2		12.6
	B	26.6		15.3
Mechanism 3 (**M3**)		**TS1**	**TSα**	**TS2**
	A	17.2	15.1	12.0
	B	26.6	15.1	12.0
	C	18.4	15.1	15.3
	D	18.4	15.1	12.6

Table S6. TSs free energies (Δ*G*, in kcal/mol) for all reaction paths computed for *meso*-B-LA propagation at **1-**(*R*)-*meso*-A-chain. In red are reported the low-lying paths following the **M1**-**M3** mechanisms with the preferred *meso*-LA enantioface (see Fig. 2-B of the main text).

meso-B propagation reaction at **1**-(*R*)-*meso*-A-chain				
Mechanism 1 (**M1**)	Path	**TS1**		**TS2**
	A	19.1		17.4
	B	23.4		13.2
	C	18.1		13.0
Mechanism 2 (**M2**)		**TS1**		**TS2**
	A	19.1		13.2
	B	23.4		17.4
Mechanism 3 (**M3**)		**TS1**	**TSα**	**TS2**
	A	19.1	14.2	13.0
	B	23.4	14.2	13.0
	C	18.1	14.2	17.4
	D	18.1	14.2	13.2

References

1 Gaussian 09, Revision D.02, Frisch, M.J.; Trucks, G.W.; Schlegel, H.B.; Scuseria, G.E.; Robb, M.A.; Cheeseman, J.R.; Montgomery, Jr., J.A.; Vreven, T.; Kudin, K.N.; Burant, J.C.; Millam, J.M.; Iyengar, S.S.; Tomasi, J.; Barone, V.; Mennucci, B.; Cossi, M.; Scalmani, G.; Rega, N.; Petersson, G.A.; Nakatsuji, H.; Hada,M.; Ehara, M.; Toyota, K.; Fukuda, R.; Hasegawa, J.; Ishida, M.; Nakajima, T.; Honda, Y.; Kitao, O.; Nakai, H.; Klene, M.; Li, X.; Knox, J.E.; Hratchian, H.P.; Cross, J. B.; Bakken, V.; Adamo, C.; Jaramillo, J.; Gomperts, R.;Stratmann, R.E.; Yazyev, O.; Austin, A.J.; Cammi, R.; Pomelli, C.; Ochterski, J.W.; Ayala, P.Y.; Morokuma,K.; Voth, G.A.; Salvador, P.; Dannenberg, J.J.; Zakrzewski, V.G.; Dapprich, S.; Daniels, A.D.; Strain, M.C.;Farkas, O.; Malick, D.K.; Rabuck, A.D.; Raghavachari, K.; Foresman, J.B.; Ortiz, J.V.; Cui, Q.; Baboul, A.G.;Clifford, S.; Cioslowski, J.; Stefanov, B.B.; Liu, G.; Liashenko, A.; Piskorz, P.; Komaromi, I.; Martin, R.L.; Fox,D.J.; Keith, T.; Al-Laham, M.A.; Peng, C.Y.; Nanayakkara, A.; Challacombe, M.; Gill, P.M.W.; Johnson, B.;Chen, W.; Wong, M.W.; Gonzalez, C.; and Pople, J.A.; Gaussian, Inc., Wallingford CT, 2004.
2 C. Lee, W. Yang and R. G. Parr, *Phys. Rev. B*, 1988, **37**, 785.
3 (a) 1 A. D. Becke, *J. Chem. Phys.*, 1993, **98**, 1372. (b) A. D. Becke, *J. Chem. Phys.*, 1993, **98**, 5648.
4 A. D. McLean and G. S. Chandler, *J. Chem. Phys.*, 1980, **72**, 5639.
5 A. Schäfer, H. Horn and R. Ahlrichs, *J. Chem. Phys.*, 1992, **97**, 2571.
6 V. Barone and M. Cossi, *J. Phys. Chem. A*, 1998, **102**, 1995.
7 S. Grimme, J. Antony, S. Ehrlich and H. Krieg, *J. Chem. Phys.*, 2010, **132**, 154104. (b) S. Grimme, *J. Comput. Chem.*, 2004, **12**, 1463.
8 M. C. D'Alterio, C. De Rosa and G. Talarico, *ACS Catal.*, 2020, **10**, 2221.
9 T. M. Ovitt and G. W. Coates, *J. Am. Chem. Soc.*, 2002, **124**, 1316.